PHYSICS OF FLUIDS **27**, 025114 (2015)

Modeling quasi-static magnetohydrodynamic turbulence with variable energy flux

Mahendra K. Verma[1,a)] and K. Sandeep Reddy[2]
[1]*Department of Physics, Indian Institute of Technology Kanpur, Kanpur 208016, India*
[2]*Department of Mechanical Engineering, Indian Institute of Technology Kanpur, Kanpur 208016, India*

(Received 7 July 2014; accepted 11 February 2015; published online 24 February 2015)

In quasi-static magnetohydrodynamics, experiments and numerical simulations reveal that the energy spectrum is steeper than Kolmogorov's $k^{-5/3}$ spectrum. To explain this observation, we construct two variable energy flux based turbulence phenomenologies. Variable energy flux is due to the Joule dissipation, which is active at all scales. In the first phenomenology, which is applicable to small interaction parameters, the energy spectrum is a power law, but with a spectral exponent steeper than −5/3. In the other limit of large interaction parameters, the second phenomenology predicts an exponential energy spectrum and flux. The predictions of the phenomenologies are in good agreement with the numerical results. © *2015 AIP Publishing LLC.* [http://dx.doi.org/10.1063/1.4913499]

I. INTRODUCTION

The liquid-metal flows in metal plate rolling and crystallization have very small magnetic Reynolds number $\mathrm{Rm} = UL/\eta$, where U, L are the large scale velocity and length scales, respectively, and η is the magnetic diffusivity. In this paper, we present several models to derive energy spectrum and flux for an idealized limit called the "quasi-static limit." In this limit, $\mathrm{Rm} \ll 1$, and the magnetic Prandtl number $\mathrm{Pm} = \nu/\eta \ll 1$, where ν is the kinematic viscosity of the fluid.

In the quasi-static limit, the induced magnetic field tends to be very small because of very large magnetic diffusivity, and it gets slaved to the velocity field that yields the Lorentz force as

$$\mathbf{F} = -\frac{\sigma B_0^2}{\rho}\left(\Delta^{-1}\frac{\partial^2 \mathbf{u}}{\partial z^2}\right), \tag{1}$$

where ρ is the density of the fluid, $\mathbf{u}$ is the velocity field, $\mathbf{B} = B_0\hat{z}$ is the external uniform magnetic field, and Δ^{-1} is the inverse of the Laplacian operator. The quasi-static approximation provides a major simplification since we do not need to solve the induction equation. The strengths of the Lorentz force and the external magnetic field are quantified using a nondimensionalized parameter called the "interaction parameter" N, which is an estimate of the ratio between the Lorentz force and the nonlinear term.

Several experimental and numerical simulations have been performed to study the energy spectrum of quasi-static magnetohydrodynamics (MHD) turbulence (see Knaepen and Moreau[1] and references therein). Kolesnikov and Tsinober[2] and Alemany *et al.*[3] performed experiments on mercury for low Rm and observed that the energy spectrum for the velocity field follows k^{-3} scaling for significantly strong interaction parameters. A similar experiment by Branover *et al.*[4] on mercury showed energy spectrum—$k^{-5/3}, k^{-7/3}, k^{-3}, k^{-11/3}$—for different interaction parameters; the exponents below −3 were attributed to the generation of helicity in the flows. In an experiment on liquid sodium, Eckert *et al.*[5] observed the energy spectrum to follow $k^{-\alpha}$, where $\alpha \in [5/3, 5]$ for interaction parameter $N \in [0.3, 1000]$.

a)Email: mkv@iitk.ac.in

Many numerical simulations of quasi-static MHD[1,6–13] show steepening of the energy spectrum with the increase of interaction parameter, similar to that seen in the experiments. It has been observed that for large interaction parameters, the flow becomes anisotropic with the energy concentrated near the plane perpendicular to the external magnetic field.[6,7,10,13–15] Recently, Reddy and Verma[6] performed simulations for interaction parameters ranging from 0 to 220, and showed that the energy spectrum is power law for $0 < N < 27$ and exponential ($\exp(-bk)$) for $N \geq 130$. Ishida and Kaneda[9] studied the modification of inertial range energy spectrum for low interaction parameters and proposed a $k^{-7/3}$ scaling law. Burattini *et al.*[12] studied anisotropy in quasi-static MHD turbulence and also observed a scaling law different from k^{-3} for the energy spectrum.

To understand these numerical and experimental findings, in this paper, we construct variable energy flux based turbulence phenomenologies for quasi-static MHD turbulence. Our phenomenologies are based on the fact that the energy flux decreases with the wavenumber due to the Joule dissipation. For interaction parameter $N \to 0$, isotropy is a good approximation for the flow. For $N \approx 1$, anisotropy starts to play a significant role in quasi-static MHD, as reported earlier in Moffatt,[16] Schumann,[17] Zikanov and Thess,[7] and Vorobev *et al.*[8] For large interaction parameters, however, the flow is highly anisotropic and has an exponential dependence on k [$E(k) \sim \exp(-bk)$]. We derived a turbulence phenomenology for small N assuming isotropy of the flow, and another one for large N using exponential form for the flux and energy spectrum. Our phenomenologies are one of the handful attempts to analytically model the quasi-static MHD turbulence. We show that results of our phenomenologies are consistent with the earlier numerical[6,12] and experimental results.[4,5] We also perform numerical simulations to validate our phenomenologies. We remark that a similar steepening of the energy spectrum was observed by Verma[18] in two-dimensional turbulence with Ekman friction.

The organization of the paper is as follows. In Sec. II, we describe the variable energy flux phenomenologies for quasi-static MHD. Section III contains details of numerical simulations used for validation of phenomenologies. Comparison between the predictions of the phenomenologies and simulation results is discussed in Sec. IV. Section V contains conclusions.

II. THEORETICAL FRAMEWORK

The governing equations for the low-Rm liquid metal flows under the quasi-static approximation are[19,20]

$$\frac{\partial \mathbf{u}}{\partial t} + \mathbf{u}\cdot\nabla\mathbf{u} = -\nabla(p/\rho) - \frac{\sigma B_0^2}{\rho}\left(\Delta^{-1}\frac{\partial^2 \mathbf{u}}{\partial z^2}\right) + \nu\nabla^2\mathbf{u} + \mathbf{f}, \tag{2}$$

$$\nabla\cdot\mathbf{u} = 0, \tag{3}$$

where $\mathbf{u}$ is the velocity field, p is the pressure field, $\mathbf{f}$ is the external force field, $\mathbf{B}_0 = B_0\hat{z}$ is the uniform external magnetic field along the z direction, σ is the electrical conductivity, ν is the kinematic viscosity, and ρ is the density of the fluid. The induction equation in Pm $\to$ 0 limit is

$$\eta\nabla^2\mathbf{b} = -(\mathbf{B}_0\cdot\nabla)\mathbf{u}, \tag{4}$$

which is the Poisson's equation, whose solution under periodic boundary condition is

$$\mathbf{b} = -\Delta^{-1}\frac{1}{\eta}(\mathbf{B}_0\cdot\nabla)\mathbf{u}. \tag{5}$$

Substitution of the above $\mathbf{b}$ in the Navier Stokes equation yields $(\mathbf{B}_0\cdot\nabla)\mathbf{b}/(\mu\rho) = (\sigma B_0^2/\rho)\Delta^{-1}\partial^2\mathbf{u}/\partial z^2$, where μ is the magnetic permittivity of the liquid metal and $\eta = 1/(\mu\sigma)$.

The corresponding equation in the Fourier space,

$$\frac{\partial \hat{u}_i(\mathbf{k})}{\partial t} = -ik_i\frac{\hat{p}(\mathbf{k})}{\rho} - ik_j\sum\hat{u}_j(\mathbf{q})\hat{u}_i(\mathbf{k}-\mathbf{q}) - \frac{\sigma B_0^2}{\rho}(\cos^2\theta)\hat{u}_i(\mathbf{k}) - \nu k^2\hat{u}_i(\mathbf{k}) + \hat{f}_i(\mathbf{k}) \tag{6}$$

is very useful in analyzing energy transfers among modes. Here, $\hat{u}(\mathbf{k})$, $\hat{f}(\mathbf{k})$ are the Fourier transforms of the velocity field and force field, respectively, and θ is the angle between the mean

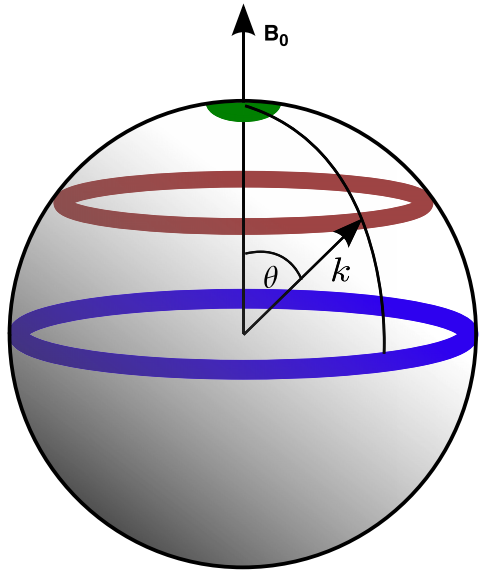

FIG. 1. Figure illustrating ring decomposition in spectral space.

magnetic field and the wavenumber **k** (see Fig. 1). The interaction parameter N is an estimate of the ratio between the Lorentz force and the nonlinear term

$$N = \frac{\sigma B_0^2 L}{\rho U}. \tag{7}$$

For large external magnetic field, N is large and flow is strongly anisotropic.

The energy equation in the Fourier space is[19,20]

$$\frac{\partial E(\mathbf{k})}{\partial t} = T(\mathbf{k}) - 2\frac{\sigma B_0^2}{\rho}\cos^2(\theta)E(\mathbf{k}) - 2\nu k^2 E(\mathbf{k}) + F(\mathbf{k}), \tag{8}$$

where $E(\mathbf{k}) = |\hat{\mathbf{u}}(\mathbf{k})|^2/2$ is the energy spectrum, $T(\mathbf{k})$ is the kinetic energy transfer rate, and $F(\mathbf{k})$ is the energy feed by the external forcing. The second and third terms on the RHS are the dissipation rates due to the Lorentz force and the viscous force, respectively. Under steady state ($\partial E/\partial t = 0$), the energy feed by $F(\mathbf{k})$ is balanced by the dissipation terms. The term $T(\mathbf{k})$ transfers energy from the large scale to small scale. In this paper, we discuss steady state properties of quasi-static MHD.

A. Variable energy flux

The zero interaction parameter corresponds to the fluid (hydrodynamic) limit. In this limit, the flow becomes turbulent when the Reynolds number $\mathrm{Re} = UL/\nu \gg 1$. In this regime, the energy spectrum exhibits the famous Kolmogorov $k^{-5/3}$ power law in the inertial range. For finite N, however, the Lorentz force induces an additional dissipation that leads to a modification of the energy flux. The variation of the energy flux due to this dissipation can be derived using the following arguments.

We assume that the energy spectrum is anisotropic due to the mean magnetic field[6,12,15] and that is described using the ring spectrum $E(k,\theta)$,[12,21] where k is the wavenumber of the ring, and θ is the angle between the mean magnetic field and the "average" wavenumber **k** of the ring, as shown in Fig. 1. We model $E(k,\theta)$ as

$$E(k,\theta) = E(k)\frac{g(\theta)}{\pi}, \tag{9}$$

where $g(\theta)$ describes the angular dependence of the energy spectrum. Integration of Eq. (9) over θ yields

$$\int_0^\pi d\theta E(k,\theta) = E(k)\int_0^\pi \frac{g(\theta)}{\pi} = E(k). \tag{10}$$

Therefore,

$$\int_0^\pi \frac{g(\theta)}{\pi} = 1. \tag{11}$$

For the isotropic case, $g(\theta) = \text{const} = 1$.

Due to the Joule dissipation, the inertial-range energy flux $\Pi(k)$ decreases with the increase of k. Quantitatively, the difference between the energy fluxes $\Pi(k+dk)$ and $\Pi(k)$ is due to the energy dissipation in the shell $(k, k+dk)$, i.e.,

$$\Pi(k+dk) - \Pi(k) = -\epsilon(k)dk = -\left\{\int_0^\pi d\theta \left[2\nu k^2 + 2\frac{\sigma B_0^2}{\rho}\cos^2\theta\right] E(k,\theta)\right\} dk \tag{12}$$

or

$$\frac{d\Pi(k)}{dk} = -\left[2c_1\nu k^2 + 2c_2\frac{\sigma B_0^2}{\rho}\right] E(k), \tag{13}$$

with

$$c_1 = \frac{1}{\pi}\int_0^\pi g(\theta)d\theta = 1, \tag{14}$$

$$c_2 = \frac{1}{\pi}\int_0^\pi g(\theta)\cos^2\theta d\theta. \tag{15}$$

In the following discussion, we construct two phenomenologies: phenomenology A for small N's for which the energy spectrum is still a power law but steeper than Kolmogorov's $k^{-5/3}$ spectrum and phenomenology B for large N for which the energy spectrum is exponential. The energy spectra and fluxes for the two cases are derived self-consistently using Eq. (13).

B. Phenomenology *A* for small interaction parameters

In the present subsection, we describe a formalism of the variable energy flux for small interaction parameters. The flow can be assumed to be approximately isotropic for $N < 1$ (to be compared via numerical simulations in Sec. IV). Therefore, we could start with Kolmogorov-like phenomenology but with a variable energy flux. Specifically, we extrapolate Pope's shell spectrum[22] for isotropic turbulence to the ring spectrum as

$$E(k,\theta) = E(k)\frac{g(\theta)}{\pi} = C[\Pi(k)]^{2/3}k^{-5/3}f_L(kL)f_\eta(k\eta)\frac{g(\theta)}{\pi}, \tag{16}$$

where C is the Kolmogorov constant with an approximate value of 1.5, $\Pi(k)$ is the energy flux emanating from the wavenumber sphere of radius k, and $g(\theta)$ is the anisotropic component of the energy spectrum. The functions $f_L(kL)$ and $f_\eta(k\eta)$ specify the large-scale and dissipative-scale components, respectively, of the energy spectrum

$$f_L(kL) = \left(\frac{kL}{[(kL)^2 + c_L]^{1/2}}\right)^{5/3+p_0}, \tag{17}$$

$$f_\eta(k\eta) = \exp\left[-\beta\left\{[(k\eta)^4 + c_\eta^4]^{1/4} - c_\eta\right\}\right], \tag{18}$$

where the c_L, c_η, p_0, β are constants. We take $C_L \approx 6.78$, $c_\eta \approx 0.40$, $\beta \approx 5.2$, and $p_0 = 2$, as suggested by Pope.[22] In the present paper, we focus on the inertial and dissipative range, hence, $f_L(kL) = 1$.

We substitute the energy spectrum of form Eq. (16) into Eq. (13), which yields

$$\frac{d\Pi(k)}{dk} = -\left[2c_1\nu k^2 + 2c_2\frac{\sigma B_0^2}{\rho}\right] C(\Pi(k))^{2/3}k^{-5/3}f_\eta(k\eta). \tag{19}$$

We integrate Eq. (19) from $k = k_1$, which is the starting wavenumber of the inertial range. Assuming that the energy flux at this wavenumber is Π_0, we obtain

$$\begin{aligned}\left[\frac{\Pi(k)}{\Pi_0}\right]^{1/3} &= 1 - \frac{2Cc_1}{3}\left(\frac{\nu^3}{\Pi_0\eta^4}\right)^{1/3} I_1(k\eta) - \frac{2c_2C\sigma B_0^2}{3\rho}\frac{\eta^{2/3}}{\Pi_0^{1/3}} I_2(k\eta)\\ &= 1 - \frac{2c_1c_3C}{3} I_1(k\eta) - \frac{2}{3}\frac{c_2CN}{\sqrt{c_3Re}} I_2(k\eta),\end{aligned} \tag{20}$$

where η is the Kolmogorov length, the dimensionless constant $c_3 = (\nu^3/\Pi_0\eta^4)^{1/3}$, and the integrals I_1 and I_2 are, respectively,

$$I_1(k\eta) = \int_{k_1\eta}^{k\eta} dk' k'^{1/3} f_\eta(k'), \tag{21}$$

$$I_2(k\eta) = \int_{k_1\eta}^{k\eta} dk' k'^{-5/3} f_\eta(k'). \tag{22}$$

We choose $c_3 = 3.1$ in order to achieve $\Pi(k) \to 0$ for $k\eta \gg 1$ when $N = 0$ (the isotropic case), and Kolmogorov's constant $C = 1.5$. We also take

$$c_1 = 1, \tag{23}$$

$$c_2 = 1/2, \tag{24}$$

which are the values when $g(\theta) = \text{const} = 1$, the isotropic case.

To compare the aforementioned phenomenological prediction with the simulations in which we force the wavenumbers $1 \le |\mathbf{k}| \le 3$, we assume that the inertial range wavenumber starts at around $k_1 = 4 \times 2\pi/L$. Therefore, the lower limit of the integral is $k_1\eta = 4(2\pi)(\eta/L) = 8\pi \times (c_3Re)^{-3/4}$. Note that the energy flux $\Pi(k)$ peaks at $k = k_1$ with value Π_0.

Equation (20) indicates that the second term, which arises due to the Lorentz force, is proportional to N. Hence, the flux decreases significantly as N is increased. The form of $\Pi(k)$ can be derived in the limiting case $\nu \to 0$, for which, in the inertial range

$$\left[\frac{\Pi(k)}{\Pi_0}\right]^{1/3} \approx 1 - \frac{c_2CN}{\sqrt{c_3Re}}\left[(k_1\eta)^{-2/3} - (k\eta)^{-2/3}\right]. \tag{25}$$

Thus, $\Pi(k)$ decreases with an increase in N.

We compute the energy spectrum using the aforementioned $\Pi(k)$

$$E(k) = \begin{cases} C\Pi_0^{2/3}k^{-5/3}f_\eta(k\eta)\left[\dfrac{\Pi(k)}{\Pi_0}\right]^{2/3}, & \text{if } k > k_1,\\ C\Pi_0^{2/3}k^{-5/3}f_L(kL), & \text{otherwise.}\end{cases} \tag{26}$$

Thus, our model predicts a variable energy flux and a steeper energy spectrum, yet a power-law spectrum. In Sec. IV A, we will compare these predictions with numerical results.

For interaction parameters above unity, the turbulence tends to be strongly anisotropic, and the energy spectrum tends to deviate strongly from Eq. (16). For $N > 1$, the flow becomes quasi-two-dimensional[6,23] and it is better to start with k^{-3} energy spectrum rather than $k^{-5/3}$. Also, for $N \gg 1$, the energy spectrum is exponential, rather than a power law.[6] These features make the above formalism inapplicable for $N > 1$. It is very difficult and cumbersome to derive a general formalism for an arbitrary value of N; however, it is quite easy to derive a phenomenology for the flows with very large interaction parameters using $E(k) \sim \exp(-bk)$. This phenomenology, termed as phenomenology B, is described in Sec. II C.

C. Phenomenology *B* for a very large interaction parameter

In phenomenology A, described in Sec. II B, we assume the energy spectrum to be a power law in k (see Eq. (16)). Numerical simulations and experiments show that this approximation is valid only for small N. For very large N, the increase of the Joule dissipation at all scales causes a rapid decrease of the energy flux, thus resulting in an exponential behavior of the energy spectrum.[6] Therefore, for very large N, it is best to take an exponential form for the energy flux, energy spectrum, and dissipation spectrum $\epsilon(k)$, since they satisfy Eq. (13). It is important to note that Reynolds number Re of the flow may be quite large, but the flow for large N is dissipative due to very strong electromotive force $\mathbf{J}\times\mathbf{B}$. The ratio of the nonlinear term and the $\mathbf{J}\times\mathbf{B}$ force can be estimated as

$$R_N = \frac{\rho U}{\sigma B_0^2 L}\frac{1}{\cos^2\theta} \sim \frac{1}{N\cos^2\theta}. \tag{27}$$

We term the above as a non-dimensional parameter based on N. For large N, $R_N \ll 1$ for $\theta \ll \pi/2$, but R_N can be quite large for $\theta \approx \pi/2$. This is the reason why we observe significant turbulence near the equator $\theta \approx \pi/2$ for large N.[6,23] The Joule dissipation dominates the viscous dissipation for large N, hence the flow is quite dissipative, even though Re is based on the ratio of the advective term and diffusion term is reasonably large. The energy is first dissipated by Joule dissipation. After this, the remaining energy, which is quite small, is dissipated by viscosity.

It is important to note that in the dissipation range of fluid or quasi-static MHD turbulence, the energy flux decreases rather sharply, but it is still nonzero. This nonzero flux is caused by the nonlinear term, without which the flux would become zero abruptly, which is not what is observed in numerical simulations (to be discussed in Sec. IV). This feature is valid for small N as well as large N. In the presence of large dissipation (e.g., for large N), small nonlinear term facilitates energy transfer from large scales to small scales.

It is important to contrast the above behaviour with that for linear Navier-Stokes, whose corresponding energy equation is

$$\frac{dE(k)}{dt} = -2\nu k^2 E(k) + F(k). \tag{28}$$

Under steady state, we obtain $E(k) = F(k)/(2\nu k^2)$ and zero Kolmogorov flux. This is clearly not the case for large N with nonzero nonlinear term. We will show in Sec. IV that the energy flux is nonzero for such cases, and it varies as $\Pi(k) \sim \exp(-bk)$.

Hence, in our quasi-static flows with large N, the nonlinear term plays a small but active role in transferring energy from the large-scale to small-scale. Fortunately, we can deduce interesting results using energy equation [Eq. (8)]. For large N, we show that $E(k) \sim \exp(-bk)$ and $\Pi(k) \sim (Pk^2 + Q)\exp(-bk)$ are exact solution of Eq. (8). These results provide new insights into the physics of dissipative quasi-static MHD.

For $N \gg 1$, we postulate that the energy spectrum and dissipation spectrum $\epsilon(k)$ follow

$$E(k) = A\exp(-bk), \tag{29}$$

$$\epsilon(k) = \frac{d\Pi(k)}{dk} = (Pk^2 + Q)\exp(-bk), \tag{30}$$

where A, P, Q, and b are parameters. Integration of Eq. (30) yields

$$\Pi(k) = \left\{P\left(\frac{k^2}{b} + \frac{2k}{b^2} + \frac{2}{b^3}\right) + \frac{Q}{b}\right\}\exp(-bk). \tag{31}$$

A comparison of Eq. (30) with Eq. (13) yields

$$P = 2Ac_1\nu, \tag{32}$$

$$Q = 2Ac_2\frac{\sigma B_0^2}{\rho}. \tag{33}$$

Thus, we show that the exponential energy spectrum and flux are consistent solutions of variable flux equation (Eq. (13)). In Sec. IV B, we verify the above predictions with numerical simulations.

We performed numerical simulations to verify the predictions of the phenomenologies described in this section. The simulation details and results are described in Secs. III and IV.

III. DETAILS OF NUMERICAL SIMULATIONS

We simulate the quasi-static MHD using pseudo-spectral method. We nondimensionalize Eqs. (2) and (3) using the characteristic velocity U_0 as the velocity scale, the box dimension L_0 as the length scale, and L_0/U_0 as the time scale and obtain

$$\frac{\partial \mathbf{U}}{\partial T} + (\mathbf{U}\cdot\nabla')\mathbf{U} = -\nabla' P - B_0'^2\left(\Delta^{-1}\frac{\partial^2 \mathbf{U}}{\partial Z^2}\right) + \nu'\nabla'^2\mathbf{U} + \mathbf{f}', \tag{34}$$

$$\nabla'\cdot\mathbf{U} = 0, \tag{35}$$

where non-dimensional variables are $\mathbf{U} = \mathbf{u}/U_0$, $\nabla' = L_0\nabla$, $T = t(U_0/L_0)$, $B_0'^2 = \sigma B_0^2 L_0/(\rho U_0)$, and $\nu' = \nu/(U_0 L_0)$.

We use pseudo-spectral code *Tarang*[24] to solve non-dimensional Eqs. (34) and (35) in a cube with 256^3 and 512^3 grids, and with periodic boundary conditions applied in all the three directions. We use fourth-order Runge-Kutta method for time-stepping, Courant-Friedrichs-Lewy (CFL) condition for calculating time-step (Δt), and the 3/2 rule for dealiasing.

We start our simulation for $N = 0$ (hydrodynamic case) by using the following energy spectrum[22] as the initial condition:

$$E(k) = C\epsilon^{2/3}k^{-5/3} f_L(kL) f_\eta(k\eta), \tag{36}$$

where the Kolmogorov constant $C = 1.5$ and $\epsilon = 1.0$. f_L and f_η are defined as

$$f_L(kL) = \left(\frac{kL}{[(kL)^2 + c_L]^{1/2}}\right)^{5/3+p_0} \tag{37}$$

and

$$f_\eta(k\eta) = \exp(-\beta k\eta), \tag{38}$$

respectively, where $c_L = 1.5$, $p_0 = 2$, and $\beta = 5.2$. The initial phases of the velocity Fourier modes are randomly generated.

In order to achieve a steady-state, we force the small wavenumber modes, which correspond to the large-scale flows. The velocity field is randomly forced in the wavenumber band $1 \le |\mathbf{k}| \le 3$, and the energy supply rate $\epsilon_{\text{in}} = 0.016$ for grid sizes 256^3 and 512^3. This scheme is similar to that followed by Burattini *et al.*,[12] Vorobev *et al.*,[8] and Carati *et al.*,[25] which is given by

$$\hat{\mathbf{f}}'(\mathbf{k}) = \gamma(\mathbf{k})\hat{\mathbf{U}}(\mathbf{k}), \tag{39}$$

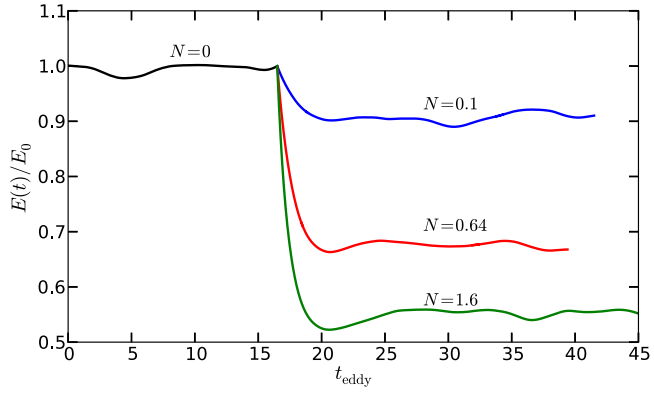

FIG. 2. Time evolution of normalized total energy $E(t)/E_0$ for different interaction parameters $N = 0$, 0.1, 0.64, and 1.6 with $k_f = [1, 3]$. E_0 is the energy at the final state of $N = 0$ simulation.

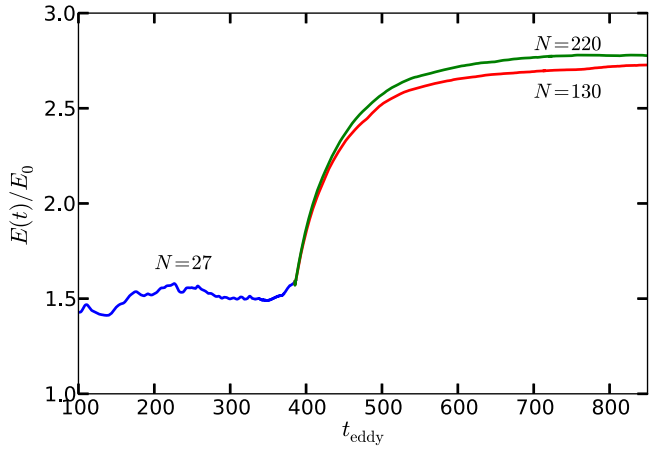

FIG. 3. Time evolution of normalized total energy $E(t)/E_0$ for $N = 27$, 130, and 220 with $k_f = [1, 3]$.

$$\gamma(\mathbf{k}) = \frac{\epsilon_{\rm in}}{n_f[\hat{\mathbf{U}}(\mathbf{k}).\hat{\mathbf{U}}^*(\mathbf{k})]}, \tag{40}$$

where n_f is the total number of modes inside the forcing wavenumber band. To simulate various interaction parameters, we vary the non-dimensional external magnetic field B_0' and fix the value of the non-dimensional viscosity ν' as 0.000 16 and 0.000 36 for grid sizes 256^3 and 512^3, respectively. The final state of $N = 0$ is used as the initial condition for $N = 0.1$, 0.64, and 1.6. We continue our simulations till another statistically steady-state is reached. In order to save computation time for large N's (130 and 220), we use the steady state of $N = 27$ as the initial condition. We have ensured that $k_{\rm max}\eta > 1.5$ for all our simulations, where $k_{\rm max}$ is the largest wavenumber of the simulation, and η is the Kolmogorov length scale. By this criteria, our simulations are well resolved.[10,26]

We simulated quasi-static MHD for interaction parameters $N = 0.1$, 0.64, and 1.6, belonging to small N regime, and for $N = 130$ and 220, belonging to the very large N limit. All the simulations were carried out till a statistical steady state is reached. The quantities shown in paper are averaged for over 12 eddy turnover times. We exhibit the evolution of energy for $N = 0.1$, 0.64, and 1.6 in Fig. 2, and that for $N = 130$ and 220 in Fig. 3. For small N, turbulence is approximately isotropic; here, the steady state of value of the global energy is lower than that for the hydrodynamic ($N = 0$)

TABLE I. Table depicting various parameters used: the grid size, non-dimensional magnetic field B_0', the interaction parameter N calculated at the steady state, the Reynolds number Re, the energy spectrum, $E_\perp/(2E_\parallel)$, non-dimensional viscosity ν', Reynolds number Re_λ based on Taylor micro-scale, c_2 of Eq. (15).

Grid	B_0'	N	Re	Scaling law	$E_\perp/(2E_\parallel)$	ν'	Re_λ	c_2
512^3	0	0	480	$k^{-5/3}$	0.99	0.000 16	140	0.35
512^3	0.739	0.10	460	$k^{-1.8}$	1.01	0.000 16	130	0.34
512^3	1.65	0.64	440	$k^{-2.0}$	1.02	0.000 16	122	0.34
512^3	2.34	1.6	370	$k^{-2.8}$	1.05	0.000 16	115	0.23
256^3	25.1	130	430	$\exp(-0.18k)$	3.0	0.000 36	126	1.4×10^{-4}
256^3	32.6	220	440	$\exp(-0.18k)$	1.7	0.000 36	128	1.3×10^{-4}

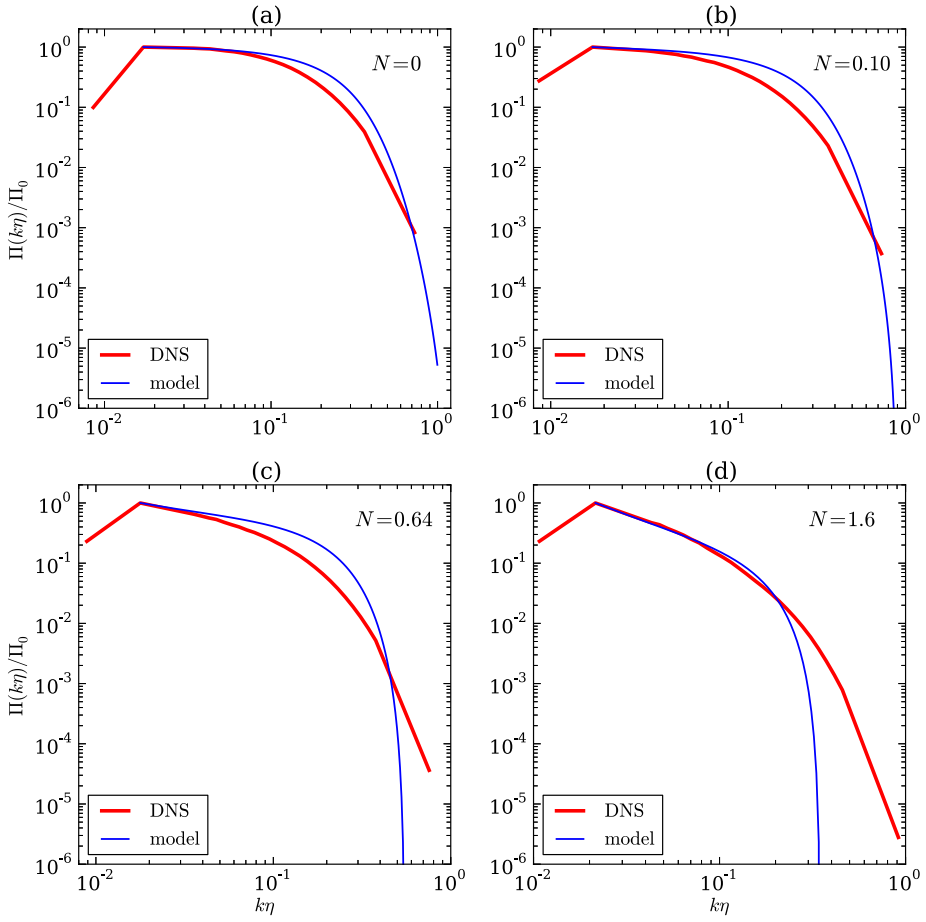

FIG. 4. Plots of normalized energy flux $\Pi(k\eta)/\Pi_0$ for (a) $N = 0$, (b) $N = 0.10$, (c) $N = 0.64$, and (d) $N = 1.6$. In all the cases, the energy flux decrease with k due to Joule dissipation.

case due to the additional Joule dissipation. However, for large N, the flow is quasi-two dimensional.[6,7,10,23] Increase in the energy level for larger N is due to the inverse cascade. Consequently, the global energy is larger than the hydrodynamic ($N = 0$) case.

The interaction parameter N for each run was computed using

$$N = \frac{B_0'^2 L}{U'}, \tag{41}$$

where U' is the root mean square (rms) of the steady-state velocity, and L is the non-dimensional integral length scale at the steady state. The Reynolds number is defined as

$$\mathrm{Re} = \frac{U'L}{\nu'}, \tag{42}$$

where U' is the rms of the velocity defined[8,12] as

$$\frac{3}{2}U'^2 = E = \int_0^\infty E(k)dk, \tag{43}$$

and L is the non-dimensional integral length scale defined as

$$L = \frac{\pi}{2U'^2}\int_0^{k_{max}} \frac{E(k)}{k}dk. \tag{44}$$

The Taylor micro-scale Reynolds number is defined as[27]

$$\mathrm{Re}_\lambda = \sqrt{\frac{15}{\nu\epsilon_\nu}}\frac{2E}{3}. \tag{45}$$

In Sec. IV, we will perform numerical simulations and compare the numerical results with the model predictions.

IV. VALIDATION OF THE PHENOMENOLOGIES USING NUMERICAL SIMULATIONS

We compute the energy spectra and fluxes for $N = 0.10$, 0.64, and 1.6 (small), as well as for $N = 130$ and 220 (large). We compare these numerical results with the predictions of the phenomenologies for verification.

A. Small interaction parameters

For a small interaction parameter, we compute the normalized energy flux $\Pi(k)/\Pi_0$ and the normalized energy spectrum $E(k\eta)/E(k_1\eta)$ using phenomenology A by substituting N in Eqs. (20) and (26), respectively. For small N, $g(\theta) \approx 1$ to a good approximation, as evident from Table I ($E_\perp/(2E_\parallel) \approx 1$ and $c_2 \approx 1/2$). In Figs. 4 and 5, we plot the normalized energy flux and spectrum, respectively.

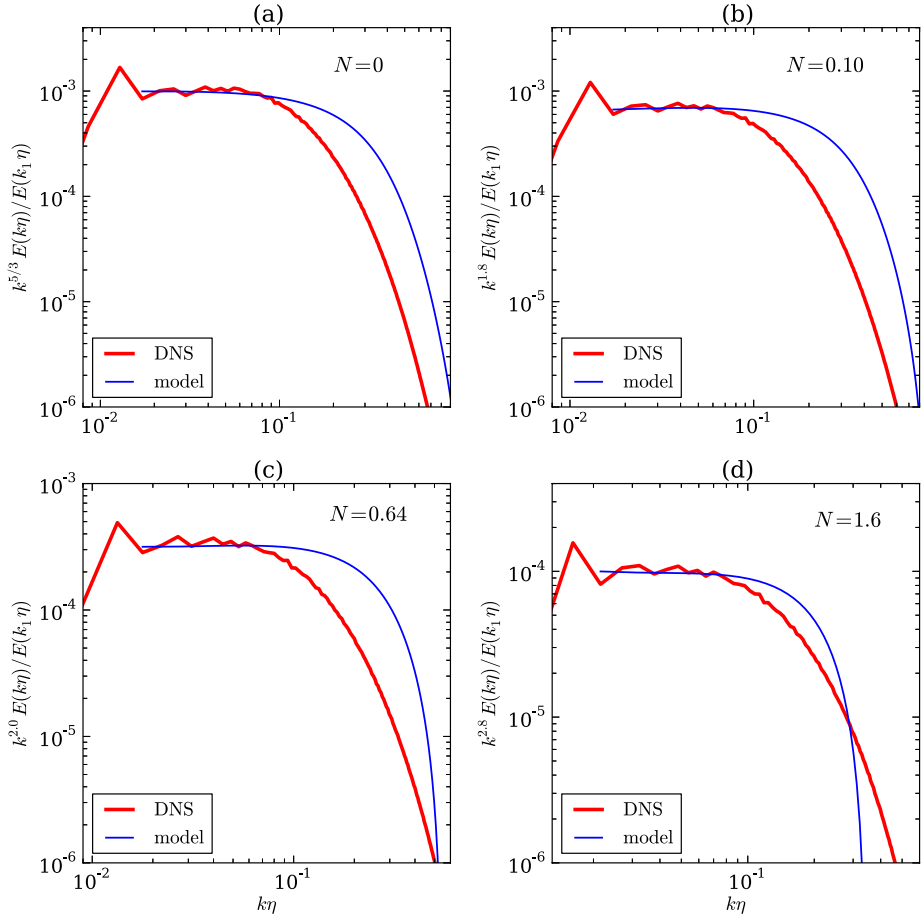

FIG. 5. Plots of compensated energy spectra $k^\alpha E(k\eta)/E(k_1\eta)$ (here, α varies with N) for (a) $N = 0$, (b) $N = 0.10$, (c) $N = 0.64$, and (d) $N = 1.6$.

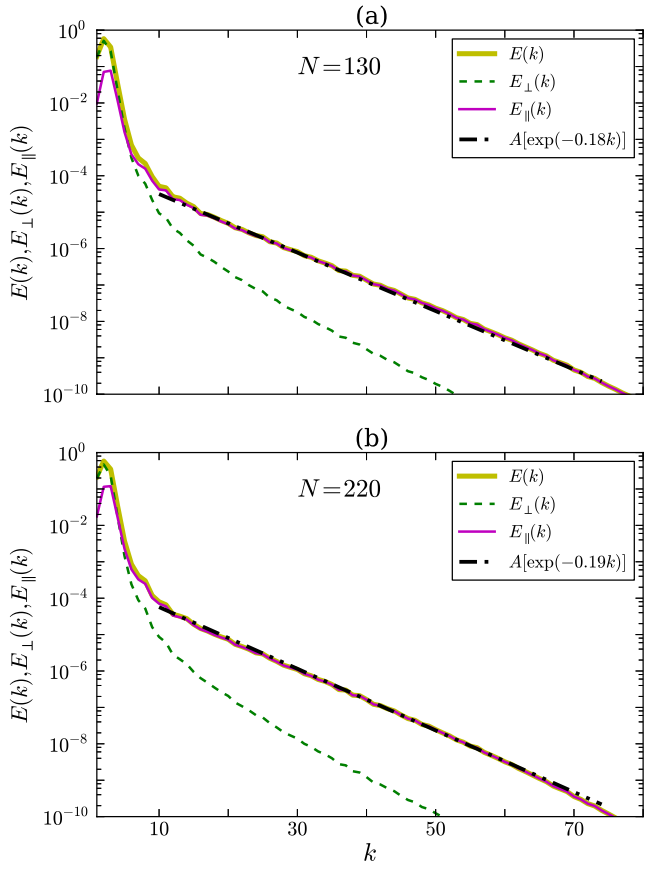

FIG. 6. For (a) $N = 130$ and (b) $N = 220$, plots of total $E(k)$, perpendicular ($E_\perp(k)$), and parallel ($E_\parallel(k)$) components of kinetic energy spectrum, respectively. The black double dot-dash is the best fit curves for $E(k)$.

To compare with the numerical results, we first compare the phenomenological predictions and numerical results for $N = 0$, which corresponds to the pure fluid. The numerical and phenomenological results, shown in Figs. 4(a) and 5(a), match reasonably well, especially in the inertial range; the energy flux is a constant, while the energy spectrum varies as $k^{-5/3}$. The agreement for the $E(k)$ of the dissipation range is not very good. However, we focus on the inertial range in this paper.

After this, we compare the numerical and phenomenological results for $N = 0.10$, 0.64, and 1.6; the energy fluxes and spectra are shown in Figs. 4(b)–4(d) and 5(b)–5(d), respectively. Figure 4 shows that for $N > 0$, the energy flux is no more constant in the inertial range, and it decreases with k. The model predictions and the numerical results are in a reasonable agreement with each other in the inertial range. The deviations between the two results in the dissipative range indicate that the function $f_\eta(k\eta)$ of Eq. (16) needs to be modified. We attempted several alternatives, e.g., an exponential function, but they appear to perform worse. A comprehensive work in this direction is required for a better agreement in the dissipative regime.

The energy spectrum shown in Fig. 5 indicates that the energy spectrum gets steeper with the increase of N. The spectral indices for $N = 0.10$, 0.64, and 1.6 are -1.8, -2.0, and -2.8, respectively, which are steeper than Kolmogorov's $-5/3$ spectral index for hydrodynamic turbulence. The trend of decreasing of the exponent of energy spectrum with increasing interaction parameter is in good agreement with earlier experimental results of Branover *et al.*[4] (see Fig. 5 of Ref. 4) and Eckert *et al.*[5] (see Fig. 10 of Ref. 5). A similar trend is also observed in direct numerical simulations (DNS) of Burattini *et al.*[12] (see Fig. 1 of Ref. 12) and Reddy and Verma[6] (see Table I of Ref. 6).

For interaction parameters far beyond unity, phenomenology A is not valid because the energy spectrum tends to be anisotropic. For moderate and large N, the flow is quasi-two-dimensional, and the spectrum may have dual power law. However, for large N, the spectrum is exponential, to be

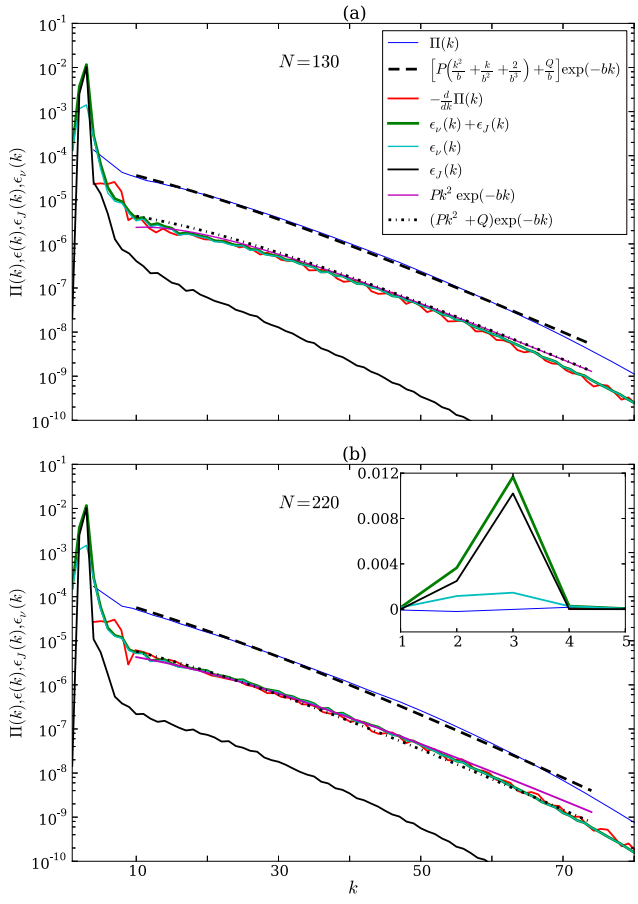

FIG. 7. For (a) $N = 130$ and (b) $N = 220$, plots of kinetic energy flux $\Pi(k)$. Note that $-\frac{d}{dk}\Pi(k) \approx \epsilon(k)$. The black dashed, dash-dot lines are the best fit curves for $\Pi(k)$ and $\epsilon(k)$, respectively.

described in Sec. IV B, where we will employ phenomenology B and compare the phenomenological predictions with the numerical results.

B. Large interaction parameters

We perform numerical simulations for $N = 130$ and 220 and compute the energy spectra, dissipation spectra, and fluxes using the steady-state data. We plot the energy spectrum in Fig. 6, and energy flux in Fig. 7. We fit the numerical results with the expressions given by Eqs. (29)-(31). As shown in Figs. 6 and 7, the model predictions for the energy spectrum and energy flux agree very well with the numerical results.

We observe that $\epsilon_J(k) > \epsilon_\nu(k)$ for $k < 6$, and vice versa. This is due to the fact that $\epsilon_\nu \propto k^2$, and $\epsilon_J(k)$ is active at all k.[23] Therefore, at large k, ϵ_ν dominates ϵ_J (see Fig. 7). In addition, we observe that $E_\perp(k) > E_\parallel(k)$ for $k < 6$ and vice versa, where $E_\perp(k)$ is the energy spectrum of the sum of the perpendicular components of the velocity, while $E_\parallel(k)$ is that of the parallel component (see Fig. 6). This is consistent with the quasi-two-dimensional behaviour of quasi-static MHD.[7,10,23]

For large N, the energy spectrum $E(k) \sim \exp(-bk)$, where $b \approx 5\eta$ and $\eta = (\nu^3/\epsilon_\nu)^{1/3}$ are the Kolmogorov's length scale, is universal for large k. Using dimensional analysis, we can argue that $E(k) \sim \exp(-bk)$ for $k > k_c = \sqrt{Q/P}$, where P and Q are present in Eq. (30). For the data given in Table II, $k_c \sim 10$. This form of $E(k)$ is valid for large k due to the fact that the ϵ_ν dominates in this range.

TABLE II. The parameters for phenomenology B, as defined in Eqs. (32) and (33), computed using the simulation data. The constants c_1, c_2 are computed using Eqs. (32) and (33), while c_2' is obtained by substituting the numerically computed $g(\theta)$ in Eq. (15).

N	b	A	P	Q	c_1	c_2	c_2'
130	0.18	2.0×10^{-4}	1.43×10^{-7}	1.7×10^{-5}	0.99	6.8×10^{-5}	1.4×10^{-4}
220	0.19	3.8×10^{-4}	2.51×10^{-7}	3.8×10^{-5}	0.92	4.7×10^{-5}	1.3×10^{-4}

We compute the parameters A, b, P, and Q using the best fit curves for the energy and dissipation spectra. These parameters are listed in Table II. We also compute the constants c_1 and c_2 by substituting these parameter values in the non-dimensionalized form of Eqs. (32) and (33),

$$P = 2Ac_1\nu', \tag{46}$$

$$Q = 2Ac_2B_0'^2, \tag{47}$$

and list them in Table II. We observe that $c_1 \approx 1$, which is consistent with Eq. (14), but c_2 differs significantly from 1/2, indicating a strong anisotropy of the flow. We also compute c_2 by substituting the numerically computed $g(\theta)$ into Eq. (15). The result, listed in Table II as c_2', is within a factor of 3 of c_2 computed using Eq. (47). Hence, the parameters are consistent with each other.

The aforementioned results shows that phenomenology B describes the energy spectrum and flux for large-N quasi-static MHD very well.

V. CONCLUSIONS

In this paper, we present two phenomenologies for quasi-static MHD. The first phenomenology, which is applicable for small interaction parameters N, predicts variable energy flux (decreasing with k) arising due to the Joule dissipation. Consequently, the energy spectrum is steeper than that of Kolmogorov's theory ($k^{-5/3}$). The phenomenology predicts that the spectral index decreases with the increase of N. The second phenomenology, for very large interaction parameters, predicts that the energy flux and spectrum are proportional to $\exp(-bk)$. The phenomenology has several parameters that are determined by the numerical or experimental data.

We have validated our phenomenological predictions with numerical simulations. We observe that the phenomenological results are in good agreement with the numerical results. We compute the parameters of the second phenomenology using the numerical data. The steepening of the energy spectrum with interaction parameter predicted by our phenomenologies is also consistent with earlier numerical simulations[6,12] and experimental results.[4,5]

Our phenomenologies, based on variable energy flux, provide valuable insights into the physics of quasi-static MHD. These phenomenologies would be very useful for understanding experimental results and in the designing of engineering applications.

ACKNOWLEDGMENTS

We are grateful to Mani Chandra for useful comments and help. We thank the anonymous referees for helpful comments. The computations were performed at the HPC system of IIT Kanpur. This work was supported by a research Grant No. SERB/F/3279/2013-14 from Science and Engineering Research Board, India.

[1] B. Knaepen and R. Moreau, "Magnetohydrodynamic turbulence at low magnetic Reynolds number," Annu. Rev. Fluid Mech. **40**, 25 (2008).
[2] Y. B. Kolesnikov and A. B. Tsinober, "Experimental investigation of two-dimensional turbulence behind a grid," Fluid Dyn. **9**, 621–624 (1974).
[3] A. Alemany, R. Moreau, P. L. Sulem, and U. Frisch, "Influence of an external magnetic-field on homogeneous MHD turbulence," J. Méc. **18**, 277–313 (1979).
[4] H. Branover, A. Eidelmann, M. Nagorny, and M. Kireev, "Magnetohydrodynamic simulation of quasi-two-dimensional geophysical turbulence," Prog. Turbul. Res. **162**, 64 (1994).

[5] S. Eckert, G. Gerbeth, W. Witke, and H. Langenbrunner, "MHD turbulence measurements in a sodium channel flow exposed to a transverse magnetic field," Int. J. Heat Fluid Flow **22**, 358–364 (2001).
[6] K. S. Reddy and M. K. Verma, "Strong anisotropy in quasi-static magnetohydrodynamic turbulence for high interaction parameters," Phys. Fluids **26**, 025109 (2014).
[7] O. Zikanov and A. Thess, "Direct numerical simulation of forced MHD turbulence at low magnetic Reynolds number," J. Fluid Mech. **358**, 299–333 (1998).
[8] A. Vorobev, O. Zikanov, P. A. Davidson, and B. Knaepen, "Anisotropy of magnetohydrodynamic turbulence at low magnetic Reynolds number," Phys. Fluids **17**, 125105 (2005).
[9] T. Ishida and Y. Kaneda, "Small-scale anisotropy in magnetohydrodynamic turbulence under a strong uniform magnetic field," Phys. Fluids **19**, 075104 (2007).
[10] B. Favier, F. S. Godeferd, C. Cambon, and A. Delache, "On the two-dimensionalization of quasi-static magnetohydrodynamic turbulence," Phys. Fluids **22**, 075104 (2010).
[11] B. Favier, F. S. Godeferd, C. Cambon, A. Delache, and W. J. T. Bos, "Quasi-static magnetohydrodynamic turbulence at high Reynolds number," J. Fluid Mech. **681**, 434–461 (2011).
[12] P. Burattini, M. Kinet, D. Carati, and B. Knaepen, "Spectral energetics of quasi-static MHD turbulence," Physica D **237**, 2062–2066 (2008).
[13] P. Burattini, M. Kinet, D. Carati, and B. Knaepen, "Anisotropy of velocity spectra in quasi-static magnetohydrodynamic turbulence," Phys. Fluids **20**, 065110 (2008).
[14] Ph. Caperan and A. Alemany, "Homogeneous MHD turbulence at low magnetic Reynolds number. Study of the transition to the quasi-two-dimensional phase and characterization of its anisotropy," Theor. Appl. Fract. Mech. **4**, 175 (1985).
[15] A. Pothérat and V. Dymkou, "Direct numerical simulations of low-Rm MHD turbulence based on the least dissipative modes," J. Fluid Mech. **655**, 174–197 (2010).
[16] H. K. Moffatt, "On the suppression of turbulence by a uniform magnetic field," J. Fluid Mech. **28**, 571–592 (1967).
[17] U. Schumann, "Numerical simulation of the transition from three- to two-dimensional turbulence under a uniform magnetic field," J. Fluid Mech. **74**, 31–58 (1976).
[18] M. K. Verma, "Variable enstrophy flux and energy spectrum in two-dimensional turbulence with Ekman friction," Eur. Phys. Lett. **98**, 14003 (2012).
[19] P. A. Davidson, *An Introduction to Magnetohydrodynamics* (Cambridge University Press, Cambridge, UK, 2001).
[20] R. Moreau, *Magnetohydrodynamics* (Kluwer Academic Publishers, Dordrecht, 1990).
[21] B. Teaca, M. K. Verma, B. Knaepen, and D. Carati, "Energy transfer in anisotropic magnetohydrodynamic turbulence," Phys. Rev. E **79**, 046312 (2009).
[22] S. B. Pope, *Turbulent Flows* (Cambridge University Press, Cambridge, UK, 2000).
[23] K. S. Reddy, R. Kumar, and M. K. Verma, "Anisotropic energy transfers in quasi-static magnetohydrodynamic turbulence," Phys. Plasmas **21**, 102310 (2014).
[24] M. K. Verma, A. Chatterjee, K. S. Reddy, R. K. Yadav, S. Paul, M. Chandra, and R. Samtaney, "Benchmarking and scaling studies of pseudospectral code Tarang for turbulence simulations," Pramana **81**, 617–629 (2013).
[25] D. Carati, S. Ghosal, and P. Moin, "On the representation of backscatter in dynamic localization models," Phys. Fluids **7**, 606–616 (1995).
[26] J. Jiménez, A. A. Wray, P. G. Saffman, and R. S. Rogallo, "The structure of intense vorticity in isotropic turbulence," J. Fluid Mech. **255**, 65–90 (1993).
[27] P. Burattini, O. Zikanov, and B. Knaepen, "Decay of magnetohydrodynamic turbulence at low magnetic Reynolds number," J. Fluid Mech. **657**, 502–538 (2010).